The Astrophysical Journal, 775:10 (12pp), 2013 September 20 doi:10.1088/0004-637X/775/1/10

BULK COMPOSITION OF GJ 1214b AND OTHER SUB-NEPTUNE EXOPLANETS

Diana Valencia[1], Tristan Guillot[2], Vivien Parmentier[2], and Richard S. Freedman[3,4]
[1] Earth, Atmosphere and Planetary Sciences Department, Massachusetts Institute of Technology, 77 Massachusetts Avenue, Cambridge, MA 02139, USA; dianav@mit.edu
[2] Observatoire de la Côte d'Azur, Université de Nice-Sophie Antipolis, CNRS UMR 7293, BP 4229, F-06300 Nice Cedex 4, France
[3] Nasa Ames Research Center, MS 245-3, P.O. Box 1, Moffett Field, CA 94035-0001, USA
[4] Seti Institute, 189 Bernardo Avenue, 100 Mountain View, CA 94043, USA
Received 2012 September 10; accepted 2013 May 2; published 2013 August 29

ABSTRACT

GJ 1214b stands out among the detected low-mass exoplanets, because it is, so far, the only one amenable to transmission spectroscopy. Up to date there is no consensus about the composition of its envelope although most studies suggest a high molecular weight atmosphere. In particular, it is unclear if hydrogen and helium are present or if the atmosphere is water dominated. Here, we present results on the composition of the envelope obtained by using an internal structure and evolutionary model to fit the mass and radius data. By examining all possible mixtures of water and H/He, with the corresponding opacities, we find that the bulk amount of H/He of GJ 1214b is at most 7% by mass. In general, we find the radius of warm sub-Neptunes to be most sensitive to the amount of H/He. We note that all (Kepler-11b,c,d,f, Kepler-18b, Kepler-20b, 55Cnc-e, Kepler-36c, and Kepler-68b) but two (Kepler-11e and Kepler-30b) of the discovered low-mass planets so far have less than 10% H/He. In fact, Kepler-11e and Kepler-30b have 10%–18% and 5%–15% bulk H/He. Conversely, little can be determined about the H_2O or rocky content of sub-Neptune planets. We find that although a 100% water composition fits the data for GJ 1214b, based on formation constraints the presence of heavier refractory material on this planet is expected, and hence, so is a component lighter than water required. The same is true for Kepler-11f. A robust determination by transmission spectroscopy of the composition of the upper atmosphere of GJ 1214b will help determine the extent of compositional segregation between the atmosphere and the envelope.

Key words: opacity – planets and satellites: composition – planets and satellites: individual (GJ 1214b, Kepler-11e) – planets and satellites: interiors

Online-only material: color figure

1. INTRODUCTION

The first step toward characterizing a planet is to infer its composition, which can only be done if at least its mass and radius are known. Within the realm of low-mass exoplanets, or super-Earths ($M < 10\,M_E$), there are now a handful of them with measured radii and masses. From internal structure models, the interpretation of the data shows two types of discovered planets: the rocky planets, including the high-density ones CoRoT-7b and Kepler-10b, with a composition similar to that of Mercury (Valencia et al. 2010; Wagner et al. 2012), and Kepler-36b with an Earth-like composition, and the "volatile" planets GJ 1214b, the Kepler-11 system, 55 Cnc-e, Kepler-18b, Kepler-36c, Kepler-68b, and Kepler-30b that are too big to be made of rocks, as well as Kepler-20b, which sits at the boundary between necessarily volatile rich and possibly rocky. These last assessments come from comparing their size to the radius of planets made of the lightest rocky composition, one devoid of iron (i.e., a planet made of magnesium silicate oxides, MgO+SiO_2). In addition, all these planets have effective temperatures that would preclude an icy composition ($T_{\rm eq} >$ 300 K). Thus, it is clear that the volatile planets have gaseous envelopes. What remains to be determined is the nature of this envelope. In particular, it is important to assess if there is hydrogen and helium as this would mean that these planets formed while the protoplanetary nebula was still around.

Several studies have looked at the problem of inferring the bulk composition of these planets, including their envelopes, through internal structure models. However, the implementation of the opacities so far has been too simple to carry out a consistent and systematic comparison between volatile compositions. These studies have taken into account the effect of composition in density (and entropy) via the equation of state (EOS), but not in the values for the opacities. The main reason for this shortcoming is that available opacity tables exist only at discrete metallicity values. Because the evolution of gaseous planets toward contraction depends on how opaque or transparent the atmosphere is, deconvolving composition and opacity values may cause an over- or underestimation of the final radius of the planet, skewing the interpretation of the data. In view of this problem, we focus on obtaining an analytical fit to the discrete Rosseland opacity tables that would allow us to interpolate to any composition spanning a hydrogen/helium + water/ices composition for the envelope.

In this study, we focus our attention on GJ 1214b, and compare its bulk composition to the other volatile planets, because it is the first low-mass planet with a measured spectrum and hence with an estimate of the composition of the upper atmosphere. Due to its size relative to its host star and the fact that the system is close enough to be bright, this planet is amenable to transmission spectroscopy. So far, several groups have obtained data at different wavelengths leading to a rough spectrum of GJ 1214b. Bean et al. (2010, 2011), Désert et al. (2011), Crossfield et al. (2011), Berta et al. (2011), and Fraine et al. (2013) have all suggested a water-dominated atmosphere or hazes to explain the featureless spectra they obtain, while Croll et al. (2011) and de Mooij et al. (2012) suggested a low-molecular weight atmosphere. One caveat of these studies is that the inferences depend on small differences between the data and the 1σ level uncertainty of the atmospheric compositional models. Increasing the uncertainty twofold would greatly impair the inference of atmospheric composition.

On the other hand, internal structure models can help constrain the bulk composition of a planet and thus complement the results from transmission spectroscopy. Two previous studies have investigated the composition of GJ 1214b. Rogers & Seager (2010b) proposed three different compositions and their respective origin for the envelope of GJ 1214b: a primordial hydrogen and helium envelope acquired while the protosolar nebula was still around, a water envelope acquired in ice form with subsequent evaporation, or a hydrogen envelope which was outgassed from the rocky interior. They used the opacity values by Freedman et al. (2008) and a static model (no contraction from the envelope) based on the parameterized gray atmospheric model by Guillot (2010). Nettelmann et al. (2011) considered the composition of GJ 1214b to be a mixture of H/He and water, with varying proportions of the two. They have an evolution model that considers cooling and contraction of the envelope, a non-gray atmospheric model, and opacities that are 50 times solar. We add to the discussion by using an internal structure model that improves on the implementation of the opacities and a comprehensive study of the possibilities for the composition of the planet.

In Section 2, we describe the structure model used and the implementation of the opacities. In Section 3, we show the results for GJ 1214b and compare them to the other volatile transiting low-mass planets. Finally, we present our summary and conclusions in Section 4.

2. MODEL

2.1. Structure and Equation of State

We treat planets as differentiated objects with an Earth-like nucleus below an envelope composed of hydrogen and helium (H/He) as well as water (H_2O). We use the combined internal structure model of Valencia et al. (2006) for the Earth-like nucleus (with composition 33% by mass iron core + 67% magnesium silicate mantle with 10% iron by mol − [($Mg_{0.9}$, $Fe_{0.1}$)SiO_3 + ($Mg_{0.9}$, $Fe_{0.1}$)O]) and CEPAM numerical model (Guillot & Morel 1995) for the gaseous envelope. The two are tied at the solid surface by ensuring continuity in mass and pressure. At this point, we have not imposed continuity in the temperature justified in part by the small effect of temperature in the density of rocks.

The EOS used is the Vinet EOS (Vinet et al. 1989) for the rocky interior by combining the EOS of the end members with the additive density rule to obtain an EOS of the mixture that is then used in the integration of the structure equations. For the envelope we use the EOS of Saumon et al. (1995) for hydrogen and helium, considering always a fixed proportion of helium by mass of 0.27 to the total amount of H_2 + He. For the water, we combine the EOS of French et al. (2009) that is relevant for temperatures above 1000 K with the NIST EOS (Saul & Wagner 1989), which is well suited for low temperatures, to span the temperature range between the critical point of water and 10,000 K.

2.2. Opacities

Owing to the fact that we are interested in constraining the composition of the envelope by spanning all possible combinations between the end members H/He and H_2O, we need corresponding opacities. Unfortunately, the data available for opacities are limited to a few discrete compositions. It is also limited in its maximal pressure, implying that interior models must rely (often implicitly) on extrapolations. We use the data from Freedman et al. (2008) updated to include revised collisional induced absorption by H_2 molecules for a solar composition, 2 and 1/2 times solar composition, plus an additional two data sets at 30 and 50 times solar (hereafter F08). We obtain an analytical fit to the Rosseland opacities by using a nonlinear least-squares minimization approach useful within the temperature and pressure ranges relevant for planetary interiors. The data sets span temperatures between 75 and 4000 K, and pressures between 10^{-6} and 300 bar, and the fit extrapolates smoothly in pressure, temperature (see Figure 1), and metallicity.

Table 1
Coefficients for Opacity Fit

	All T		$T < 800$ K	$T > 800$ K
c_1	−37.50	c_6	−14.051	82.241
c_2	0.00105	c_7	3.055	−55.456
c_3	3.2610	c_8	0.024	8.754
c_4	0.84315	c_9	1.877	0.7048
c_5	−2.339	c_{10}	−0.445	−0.0414
		c_{11}	0.8321	0.8321

The analytical fit has the form for the opacity $\kappa_{\rm gas}$ (in g cm^{-2})

$$\kappa_{\rm gas} = \kappa_{\rm lowP} + \kappa_{\rm highP} \quad (1)$$

$$\log_{10}\kappa_{\rm lowP} = c_1(\log_{10} T - c_2 \log_{10} P - c_3)^2 + (c_4\,{\rm met} + c_5) \quad (2)$$

$$\log_{10}\kappa_{\rm highP} = (c_6 + c_7 \log_{10} T + c_8 \log_{10} T^2) + \log_{10} P\,\left(c_9 + c_{10}\log_{10} T\right) + {\rm met}\, c_{11}\left(\frac{1}{2} + \frac{1}{\pi}\arctan\left(\frac{\log_{10} T - 2.5}{0.2}\right)\right), \quad (3)$$

where T is the temperature in kelvin, P is the pressure in dyn cm^{-2}, and met is the metallicity with respect to solar in the logarithmic scale (i.e., met = [M/H]). This fit effectively transitions smoothly between two different functions that are relevant at low ($\kappa_{\rm lowP}$) and high pressures ($\kappa_{\rm highP}$), respectively. The values for the coefficients are shown in Table 1. Figure 1 shows a comparison between the data from F08 for a solar composition and a metallicity 30 times higher ([M/H] = 1.5) and the results from our proposed analytical fit.

The calculations by F08 consider a grain-free atmosphere with a composition that evolves depending on the condensates that form and get removed from the gaseous phase. We are interested in assessing whether or not grains have an impact on the inference in envelope composition. We focus on the end-member case of refractory grains not settling into clouds, but remaining mixed within the background gas. To model this type of grains we turn to the calculations by Alexander & Ferguson (1994, hereafter AF94) to come up with a simple prescription that includes the opacity contribution from mixed grains. Alexander & Ferguson (1994) examined opacities at warm to high temperatures (between 700 and 12,500 K), and low-density values captured in $\log_{10}\bar{R} = -7$ to +1 where $\bar{R} = \rho/T_6^3$, ρ is the density in g cm^{-3}, and T_6 is the temperature expressed in millions of degrees (corresponding densities are 10^{-15} to 10^{-8} g cm^{-3} at 1000 K and 10^{-13} to 10^{-5} g cm^{-3} at 10,000 K) most relevant to the conditions of the protoplanetary

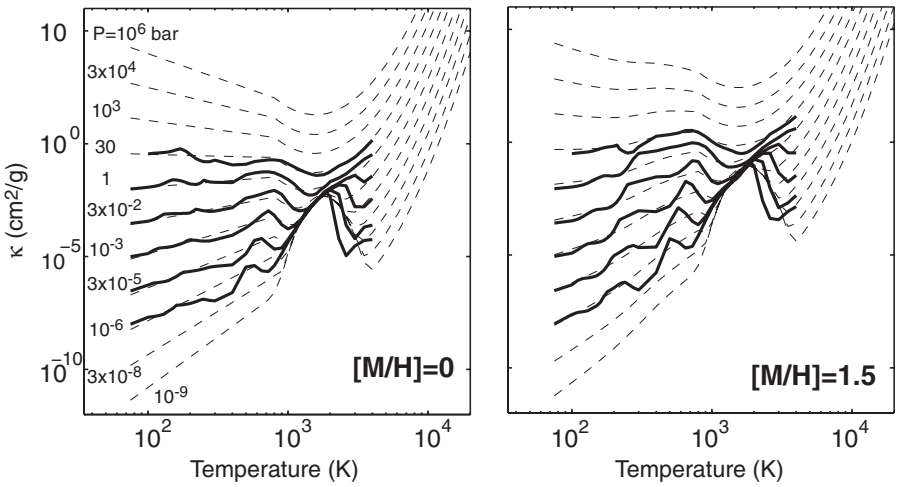

Figure 1. Opacity fit. The comparison between the Rosseland opacity data by Freedman et al. (2008) (solid lines) and our analytical fit (dashed lines) is shown for solar metallicity (left) and a metallicity 30 times higher than solar (right). The extrapolation to low and high pressures as well as large temperatures is smooth.

nebula. In contrast, planetary interiors have larger density/pressure so that typical values are $+6 < \log_{10} \bar{R} < +7$. Their results show that grains are only present below a certain temperature, which depends on the value of $\bar{R}$. Despite the fact that AF94's data are calculated at very low values of $\bar{R}$, there is a clear trend on the effect of grains that we extrapolate to larger values of $\bar{R}$ (see Figure 6 in Alexander & Ferguson 1994). We fit a simple linear trend within the regions where grains are present and add this to the gas opacity:

$$\kappa = \begin{cases} \kappa_{\rm gas} + \kappa_{\rm grains} & \text{if } T < T_1^*, \text{ and} \\ \quad \log_{10} \kappa_{\rm grains} = 0.430 & \\ \quad\quad +1.3143(\log_{10} T - 2.85) & \\ \kappa_{\rm gas} & \text{if } T > T_2^*, \end{cases} \tag{4}$$

where $\log_{10} T_1^* = 0.0245 \log \bar{R} + 1.971$ and $\log_{10} T_2^* = 0.0245 \log \bar{R} + 3.221$. The region between these two critical points is just a linear interpolation between $\kappa_{\rm gas}(T_1^*) + \kappa_{\rm grains}(T_1^*)$ and $\kappa_{\rm gas}(T_2^*)$.

We show the comparison between the two data sets (from AF94 and F08) and our fit to the data with a prescription for grains at low temperatures (dashed lines) and without grains (dotted lines) in Figure 2. On the left, we compare the data (thin lines for AF94, thick lines for F08) and our fit (dashed) for low densities ($\log_{10} \bar{R} = -1$ (black) and $\log_{10} \bar{R} = +1$ (blue)) and a solar composition. According to AF94, the majority of the opacities for temperatures lower than T_2^* (or ~1800 K for $\log_{10} \bar{R} = +1$) are due to grains, which we account for. The second feature of AF94 is a modest increase (a "bump") in the opacities due to the presence of water vapor at temperatures right above T_2^* (between 1800 K and 3000 K for $\log_{10} \bar{R} = -1$), which becomes less prominent with increasing value of $\bar{R}$ (Alexander & Ferguson 1994). We note that this feature is missing in our fit to the data by F08 yielding differences in the opacities of almost an order of magnitude around the 10^{-2} cm^2 g^{-1} level within this high-temperature and low-pressure (e.g., low $\bar{R}$) range. However, this mismatch we think may be less of an issue at pressure–temperature values pertinent to planetary interiors given that the trend is for this feature to be less prominent with increasing $\bar{R}$ values, and that the opacities relevant for planetary atmospheres are in the 1–10^6 mag range.

We compare the effect of envelope composition by showing in Figure 2 (right) the opacities for a solar ($Z_{\rm ices} = 0.01$, where $Z_{\rm ices}$ is the ratio of water/ices to envelope mass, pink), a 50% H/He + 50% H_2O/ices mixture ($Z_{\rm ices} = 0.5$, purple), and a 100% H_2O/ices envelope ($Z_{\rm ices} = 1$, blue) at a constant, more relevant value of $\log_{10} \bar{R} = +6.5$. It can be seen that the opacities increase smoothly and monotonically without grains (solid lines). In the presence of grains there is a considerable (almost step-like) increase in opacities for temperatures below ~2000 K that depends on how much water there is, from more than 1 order of magnitude for solar composition to just a few tens of dex for envelopes rich in water/ices. The small effect of grains on water-rich atmospheres is due to the fact that the opacities are already quite high for such compositions.

We find that very quickly the opacities become high as soon as the envelopes have non-negligible amounts of water/ices so that the difference between opacities for a 50× solar envelope (or $Z_{\rm ices} = 0.25$) and a pure water/ices is only of the order of ~50 g cm^{-2} over a range that covers several orders of magnitude (see Figure 2).

Extrapolation. The pressure–temperature regime of super-Earths is between millibars to a few megabars, and between a few hundred to ~10,000 K. The opacity database from which the fit is derived covers this regime partially, and extrapolation is needed beyond 300 bar and 4000 K (Figure 1). In fact, no current database covers the planetary regime fully. Therefore, internal structure studies of planets use some sort of extrapolation. We used the work by AF94 to serve as a guide for the extrapolation to high temperatures, and note that the opacities become increasingly more uncertain as the pressures and temperatures increase much beyond the database of AF08. This may not be too much of a problem as the high PT regime corresponds to the deep interior of the planet (which is fully convective), and most of the cooling is controlled by the radiative upper part of the envelope/atmosphere ($P <$ kbar, $T < 2000$ K), where the opacities are either not too far from or within the database range. However, it is important to keep in mind the limitations of the extrapolation.

In general, the construction of high-temperature databases requires that transitions that originate in energy levels above the ground state be included in the calculations. If this is not done, then there will be missing opacity that will increase in magnitude as the temperature increases. In the case of the opacity tables provided for this study, wherever possible opacity data using "hot" line lists have been used. These lists include

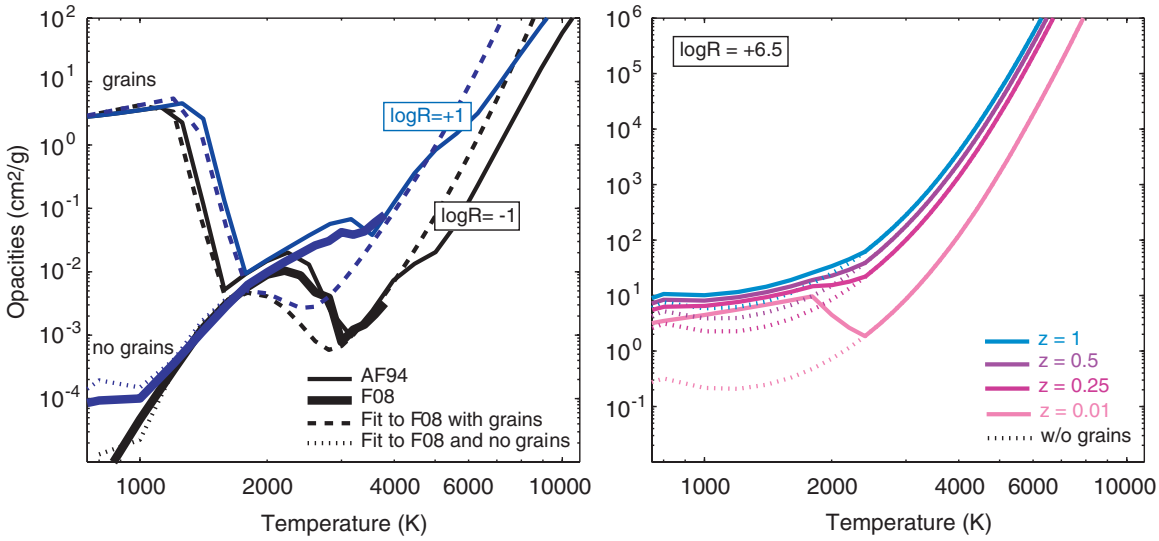

Figure 2. Comparison opacities. Left: for a solar composition, opacities according to Alexander & Ferguson (1994) are shown in thin solid lines, according to Freedman et al. (2008) in thick solid lines, our fit with grains in dashed lines and without grains in dotted lines at $\log_{10} \bar{R} = -1$ in black and $\log_{10} \bar{R} = +1$ in blue. Right: comparison for three different envelope compositions: solar, $Z_{\rm ices} = 0.01$, pink; 50% ices + 50% H/He, $Z_{\rm ices} = 0.5$, purple; and pure ices, $Z_{\rm ices} = 1$, blue for $\log_{10} \bar{R} = +6.5$ (relevant to planetary interiors) and grainy (solid) and grain-free (dotted) cases. Our fit is an extrapolation of the data beyond 4000 K, 300 bar, and $Z_{\rm ices} = 0.25$.

line transitions from levels that are not populated at room temperature so that the opacity is more accurately represented at higher temperatures, but these lists still may not include all the opacity at the highest temperatures. It is difficult to include in a quantum-mechanical model all the levels that may contribute opacity at the highest temperatures.

By considering the species individually and assessing how they contribute to the total opacity, it is reasonable to assume that the opacity will continue to increase with T but only up to the point where the population of the upper states reaches a limit where the effects of additional increases in T are slight (due to the exponential dependence of the Boltzmann factor). Since for most polyatomics the first excited electronic state is far above the ground state, it is only the vibrational/rotational levels in the ground electronic state that need to be considered. This is especially true in the case of a main source of opacity, water, where the first bound, excited state is ~7.5 eV above the ground state. On the other hand, an important source of absorption at high T is the presence of free electrons and the associated free–free and bound–free opacities, which may have a more significant effect than the filling of the band gaps, counteracting the saturation effect previously discussed.

In addition, the effect of very high pressure may also have a leveling-off component. For moderate pressures, the line width will increase with pressure, but eventually a limit is reached when the density approaches a value where the gas starts to behave more like a liquid and the line width no longer increases linearly with pressure. Unfortunately, the actual line width at these high pressures is not at all well known and the simple theories for line shape are no longer valid, making extrapolation rather uncertain.

To test how sensitive the extrapolation is to high temperatures we use a synthetic opacity fit with a much lower dependence on temperature (parameter $c_8 = 5$). We consider two planets with a mass of 0.020 $M_{\rm Jup}$, $T_{\rm eq} = 500$ K, and a core mass fraction of 50%: one with a 100% water/ices envelope and one with a mixture of 90% H/He and 10% water/ices. We find that the radiative–convective boundary moves shallower by 10% and 20% in pressure at 10 Gyr, respectively, and that the opacity values increase by 12% and 17%, respectively—not enough to change the PT structure or total radius significantly (by 0.2% and 5%, respectively, at 2.5 Gyr and by less than 1 part in 1000 for both cases at 10 Gyr). This confirms that the PT regime for the opacities is most important up to the pressures and temperatures that include the radiative–convective transition, which for these warm sub-Neptunes is <5 kbar and <2000 K.

In addition, the database used (AF08) only spans a limited range of envelope compositions: solar, 1/2× solar, 2× solar, 30× solar, and 50× solar in gaseous form (no solids). Thus, extrapolation is needed to cover the whole space from solar to water-rich envelopes. From this set we observe that the dominant dependence of the logarithm of the opacity with metallicity is a linear dependence beyond some estimated temperature (~3000 K). This simple fit (see Equation (3)) captures the intuitive behavior that opacity increases with the number of molecules present, while fitting the database well. It is, of course, too simple of an extrapolation to capture the details. We await actual data at larger metallicity values to compare to our fit, especially as more sub-Neptune planets are found.

We hope that in the future there will be no need for extrapolation, and we encourage the expansion of opacity databases to higher PT and water-rich compositions, as they are important for modeling the structure of low-mass exoplanets; in the meantime our proposed fit may serve as a starting point.

2.3. Metallicity and Composition

To use the opacity fit, we relate the composition of the envelope to metallicity. We consider the envelope to be composed of H_2–He and "ices," where the ices are composed of water, ammonia, and methane ($H_2O + NH_3 + CH_4$), in the same proportions as in the solar nebula. We implicitly assume that there are no rock-forming minerals that could bind to oxygen, so that the amount of water in the envelope is reflected in the amount of oxygen atoms (N_O), and that the other ices are fixed by the solar ratios of carbon and nitrogen to oxygen.

This means that $Z_{\rm ices}$, the amount of "ices" by mass, is

$$Z_{\rm ices} = \frac{N_{\rm O}\mu_{\rm H_2O} + N_{\rm C}\mu_{\rm CH_4} + N_{\rm N}\mu_{\rm NH_3}}{N_{\rm H}\mu_{\rm H} + N_{\rm He}\mu_{\rm He} + N_{\rm O}\mu_{\rm O} + N_{\rm C}\mu_{\rm C} + N_{\rm N}\mu_{\rm N}},$$

where N_i and μ_i are the number of atoms and the molecular weight of species i, respectively. We take constant the proportion of He to the total amount of mass in the non-metallic portion (H_2+He) and equal to $c = 0.27$ (i.e., using the conventional notation: $Y/(X+Y) = 0.27$). Therefore, the metallicity can be expressed as

$$\left(\frac{N_{\rm O}}{N_{\rm H}}\right) = \left(\frac{1}{1-c}\right)\frac{\mu_{\rm H}\, Z_{\rm ices}}{a - b\, Z_{\rm ices}}$$

$$10^{\rm met} = \left(\frac{N_{\rm O}}{N_{\rm H}}\right) \Big/ \left(\frac{N_{\rm O}}{N_{\rm H}}\right)_{\rm solar},$$

where $a = \mu_{\rm H_2O} + (N_{\rm C}/N_{\rm O})\,\mu_{\rm CH_4} + (N_{\rm N}/N_{\rm O})\,\mu_{\rm NH_3}$, and $b = (\mu_{\rm O} - 2c(\mu_{\rm H}/1-c)) + (N_{\rm C}/N_{\rm O})(\mu_C - 3c(\mu_{\rm H}/1-c)) + (N_{\rm N}/N_{\rm O})(\mu_{\rm N} - 4c(\mu_{\rm H}/1-c))$. We used the values of $N_{\rm C}/N_{\rm O} = 0.501$, $N_{\rm N}/N_{\rm O} = 0.138$, and $(N_{\rm O}/N_{\rm H})_{\rm solar} = 4.898\times10^{-4}$ from Lodders (2003). This means that our opacity fit spans values for the metallicity from solar to 457 times solar (met = 2.66), corresponding to $Z_{\rm ices} = 1$.

2.4. Atmospheric Model

The upper boundary condition of our interior model is given by the atmospheric model of Guillot (2010). This analytical model is valid for a plane–parallel atmosphere which transports both a thermal intrinsic flux and a visible flux from the star. The visible flux propagates downward from the top of the atmosphere and is absorbed with an opacity $\kappa_{\rm v}$. The ratio of the visible to the infrared opacities $\gamma \equiv \kappa_{\rm v}/\kappa_{\rm IR}$ is considered constant. Its value determines at which depth the radiative energy from the star is deposited. For high values of γ, the energy is deposited in the upper layers of the atmosphere and can be lost toward space very easily. For values of γ lower than unity, the energy is deposited in deeper layers, where the atmosphere is optically thick in the infrared. There, the energy cannot escape the planet, and contributes to its global energy, slowing its contraction. Theoretically, γ could be calculated from the opacity tables. However, we note that the temperature of the isothermal zone around the 1 bar level is very sensitive to its value. Thus, we use the value of γ that better reproduces the more sophisticated radiative transfer models of Miller-Ricci & Fortney (2010). We choose $\gamma = 0.032$, which gives a temperature of 1000 K around 1 bar for GJ 1214b, as can be seen in Figure 3. Miller-Ricci & Fortney (2010) show that, in the case of GJ 1214b, the temperature around 1 bar does not depend strongly on the composition of the planet. Thus, we use the same γ for the different compositions considered. For GJ 1214b, we find that the interior temperature is 62 K at 0.1 Gyr, 40 K at 1 Gyr, 35 K at 2.5 Gyr, and 24 K at 10 Gyr for a solar atmosphere, and 80 K at 0.1 Gyr, 50 K at 1 Gyr, 42 K at 2.5 Gyr, and 35 K at 10 Gyr for a water-rich envelope.

Note that γ will change with orbital distance. It is expected to be higher for planets that are close-in. The Rosseland opacities are calculated from the line-by-line opacities weighted by the Planck function. Thus, planets with different equilibrium temperatures have different values of the Rosseland thermal opacities. Changing the equilibrium temperature by a small amount ($\sim O(100\,{\rm K})$) will not change the position of the peak of the Planck function very much. However, for hotter planets, not considered in this study, the value of gamma could change significantly.

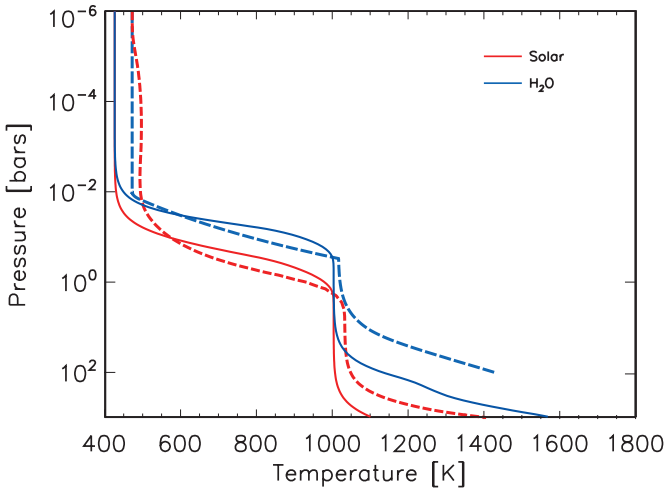

Figure 3. Upper atmosphere of GJ 1214b. Temperature pressure profiles from Miller-Ricci & Fortney (2010) (thin lines) and from our model at 10 Gyr (thick lines) for a solar composition atmosphere (red) and for a water atmosphere (blue).

(A color version of this figure is available in the online journal.)

3. RESULTS

3.1. GJ 1214b

We obtain the structure and total radius for planets with a mass of 5.09, 6.36, 7.63, 8.90, and 10.2 $M_{\rm Earth}$ (or 0.016, 0.020, 0.024, 0.028, and 0.032 $M_{\rm Jup}$) to span the mass of GJ 1214b, for different proportions of Earth-like nucleus to envelope, while spanning all combinations of the end members H/He and H_2O for the envelope. In other words, we find a relationship between mass (M), radius (R), Earth-like nucleus fraction to total mass (nf), and proportion of water to total envelope mass (wf), in the form $R = R(M, {\rm nf}, {\rm wf})$, and spline interpolate in the three dimensions (mass, nf, wt). Since we are interested in inferring the composition of a planet from its transit radius, we consider the radius of the planet to be the height at which the path traveled by the starlight would be equal to an optical depth of unity. We examined three cases: (1) a grain-free envelope, (2) a grainy envelope at an equilibrium temperature of $T_{\rm eq} = 500$ K, and (3) a grain-free envelope at $T_{\rm eq} = 600$ K.

Figure 4 shows typical calculations for the planets considered. In this case, the planets have an Earth-like nucleus that makes up half of the planet's mass below envelopes of different compositions: (1) 100% H_2O (blue), (2) 50% H_2O+ 50% H/He (purple), and (3) 100% H/He (pink). Starting from a high entropy state (corresponding to $S = S(\chi_{\rm env}, T_{10}, P_{10})$, where $\chi_{\rm env}$ is the envelope's composition, T_{10} and P_{10} are the temperature and pressure at 10 bar), the planets cool and contract according to how much energy is being transported out (bottom left panel). The solid and dashed lines correspond to equilibrium temperatures of 500 and 600 K. As can be seen, this small difference in equilibrium temperature has little effect on the interior structure or evolution of the planets.

Not surprisingly, the envelopes that have lower molecular weight yield the largest radii, while at the same time suffer the most contraction. We find this trend to be true for most planets except for the ones that have less than 10% content of water in the envelope. That is to say, we find that planets that have envelopes of 100% H/He are slightly smaller than

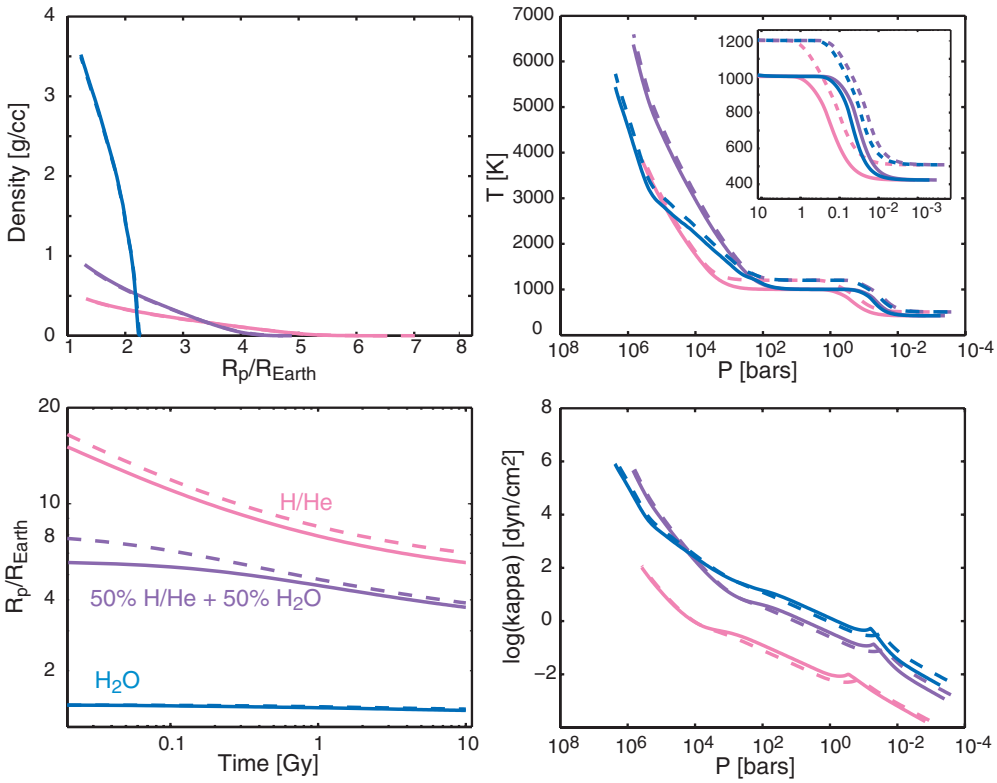

Figure 4. Envelope structure of a sub-Neptune. Top left: density structure; top-right: pressure–temperature structure; bottom left: evolution (contraction) tracks; and bottom right: opacity values for planets that are made of 50% by mass Earth-like core below envelopes of different compositions. Blue: 100% H_2O envelopes; purple: 50% H_2O + 50% H/He; pink: 100% H/He envelope. Solid and dashed lines correspond to equilibrium temperatures of 500 and 600 K, respectively. The envelopes are grain-free in this case. The total mass of the planet is 0.020 $M_{\rm Jup}$.

those that have 90% H/He+10% water/ices envelopes. We attribute this to a competing effect between larger envelope density that would make planets smaller for a given mass and higher opacities that slow down the cooling. At larger fractions of water content in the atmosphere, the density effect dominates. Interestingly, this effect gives rise to a new kind of degeneracy. For the same value of envelope mass, two different combinations of H/He + water/ices with two different evolutionary tracks yield the same radius at some given age (see Figure 5). This illustrates the importance of using evolutionary models, as static ones could miss these possibilities. By implementing the physics behind contraction and evolution, the internal structure model is able to resolve time-dependent possibilities. This degeneracy stands in contrast to the one that arises from trade-offs between three or more compositional end members with different molecular weights—iron cores, silicate mantles, water/icy envelopes or oceans, H/He envelopes—which has been readily identified (Valencia et al. 2007; Adams et al. 2008; Rogers & Seager 2010a). The new degeneracy arises from differences in molecular weight and thermo-physical properties (opacities) between water and H/He that determine the cooling histories of the envelopes.

For the specific example shown in Figure 5, a planet with a mass of 0.020 $M_{\rm Jup}$ and an envelope that makes up 3% of the total mass, two different envelope compositions yield the same radius of 6.55 $R_{\rm E}$ at 3 Gyr: an envelope that is mostly H/He (99.9% H/He and only 0.1% water in the envelope) that starts very expanded and contracts rapidly initially, and an envelope that is made of 3/4 of H/He and 1/4 of water that contracts initially more slowly. To resolve this kind of degeneracy one would need a radius measurement at two different ages, which

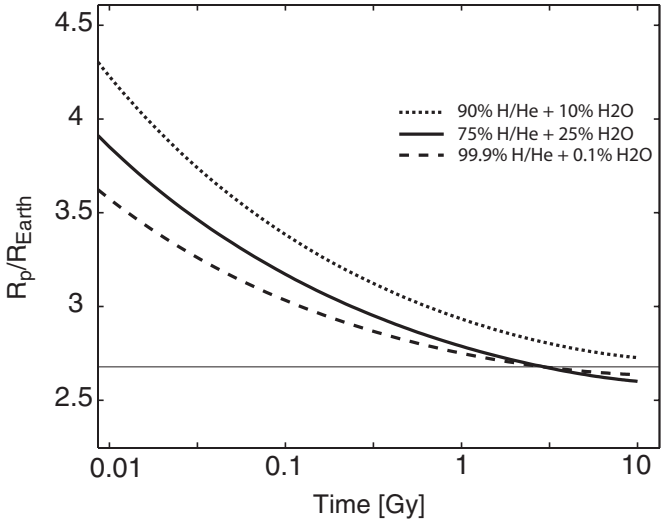

Figure 5. Degeneracy in envelope composition. Evolutionary tracks are shown for a planet of mass 0.020 $M_{\rm Jup}$ and $T_{\rm eq}$ =500 K, with an envelope that is 3% by mass and different compositions: 75% H/He + 25% H_2O (solid line), 99.9% H/He + 0.1% H_2O (dashed line), and 90% H/He + 10% H_2O (dotted lines). The latter is shown for reference. The radius of 6.55 $R_{\rm E}$ is met by the first two compositions at an age of ∼3 Gyr (fine horizontal line).

is impossible to obtain. Therefore, we find that for low-mass planets with a non-negligible envelope or sub-Neptunes, there is an intrinsic and persistent degeneracy that stems from the contraction history of the planet.

The age of GJ 1214b is estimated to be between 3 and 10 Gyr (Charbonneau et al. 2009), which means the planet may contract

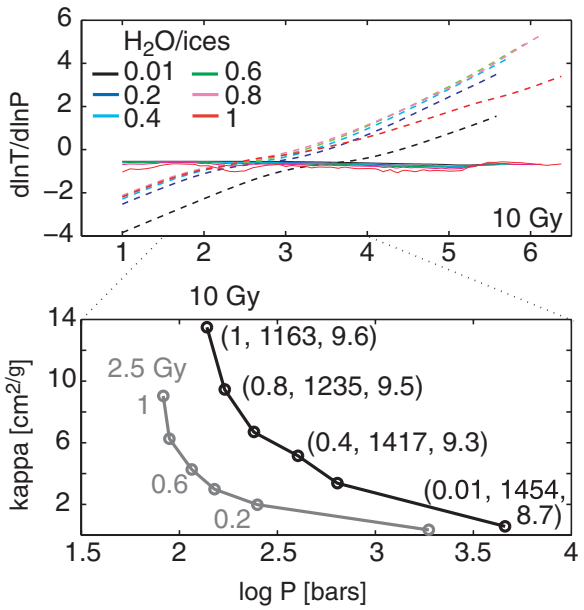

Figure 6. Adiabatic–radiative boundary of a sub-Neptune with mass 0.020 $M_{\rm Jup}$ and $T_{\rm eq}$ =500 K. Top: adiabatic (solid lines) and radiative (dashed) gradients at 10 Gyr of envelopes with compositions: solar (black), 80% H/He + 20% H_2O/ices (blue), 60% H/He + 40% H_2O/ices (cyan), 40% H/He + 60% H_2O/ices (green), 20% H/He + 80% H_2O/ices (pink), 100% H_2O/ices (red), over an Earth-like nucleus that makes 50% of the planet by mass. In the region where the radiative gradient is lower than the adiabatic one, the planet loses heat via radiation. Bottom: the pressure (depth) and corresponding opacity of the radiative–convective boundary for planets of 2.5 Gyr (gray) and at 10 Gyr (black). The labels correspond to the proportion of H_2O/ices in the envelope, and the temperature and entropy (in log) of the radiative–convective boundary. For 2.5 Gyr these values are (0.01, 1478, 8.7), (0.2, 1438, 9.1), (0.4, 1391, 9.3), (0.6, 1357, 9.4), (0.8, 1278, 9.5), (1, 1211, 9.6); and for 10 Gyr: (0.01, 1454, 8.7), (0.2, 1452, 9.1), (0.4, 1417, 9.3), (0.6, 1307, 9.4), (0.8, 1235, 9.5), (1, 1163, 9.6).

considerably within this age range, adding another source of uncertainty when inferring the composition of the envelope. The effect of contraction is most significant in the early stages of evolution (<1 Gyr) and for H/He dominated envelopes, and less important as the age of the planet increases or its envelope is H_2O dominated. These two effects are shown in the bottom left panel of Figure 4. To infer the composition of GJ 1214b, we use a nominal age of 4.6 Gyr and then explore the effects of the uncertainty in the age.

Heat is normally transferred out of the planet's envelope by convection in the interior where the adiabatic gradient is lower than the radiative one, and by radiation in the upper layers where the opacity is lower and the converse is true. We find that this radiative–convective boundary happens at deeper levels, larger temperatures, and lower local entropies, as the amount of water+ices in the envelope decreases (see Figure 6). The variation in opacity and pressure of this boundary is at least an order of magnitude and decreases with increasing water+ice content (from 4600 bar for a solar composition to 138 bar for a water/ice envelope). In addition, with increasing age this boundary happens at a similar local entropy, which means it moves deeper (higher pressures) as the planet cools in time. Below the boundary, the envelope is fully adiabatic and the values for opacities are less important, as long as they do not preclude the envelope from being convective. This means that the extrapolation of the opacities is most important up to several kilobars (∼5000 bar) and a few thousand kelvin (∼2000 K) for these warm sub-Neptune planets.

The effect of grain opacity is shown in Figure 7, where we present the results for the transit radius corresponding to two different envelope compositions: (1) 100% H_2O, (2) 50% H_2O+ 50% H/He, while also changing the proportion of envelope to Earth-like nucleus. The effect of grains (dash-dotted lines) is most noticeable for low molecular weight atmospheres and is negligible for water-dominated envelopes. This is because for water-dominated atmospheres the gas opacities are already high (∼10 g cm^{-2}) and comparable to the grain opacities (within a factor of ∼0.5 dex), while for H/He dominated atmospheres the gas opacity is 0.1–1 g cm^{-2}, one order of magnitude smaller than with grains (compare solid and dotted pink lines in Figure 2).

It is important to note that the mass and radius data for GJ 1214b are consistent with a pure H_2O/ices composition (see Figure 7(left)), regardless of the uncertainty in age, as contraction is negligible for water-dominated atmospheres. However, this composition is unlikely to exist. The condensation temperature of water and ices is much lower than that of rocks, so that during condensation some refractory material should have condensed out of the solar nebula before the bulk of the water and ices did, entailing the existence of some amount of rocky material in this planet. This, in turn, implies the presence of a material lighter than water as well, so as to offset the high-density character of the refractory material and fit the radius of the planet. The most obvious component is H/He because of its abundance in astrophysical objects, although another possibility is outgassed hydrogen (Rogers & Seager 2010b).

The effect of temperature is very small for super-Earths but modest for sub-Earths (see Figure 7). It is in fact comparable to the effect of grains, which is more important for low molecular-weight envelopes. Relevant to GJ 1214b we can quantify the effect of equilibrium temperature by noting that a 100 K increase in equilibrium temperature (that translates to an increase of ∼200 K at 10 bar) increases the radius of the planet by only ∼2%. The temperature effect is small as long as the species in the envelope do not change phase with different equilibrium temperatures.

More systematically, we ran the internal structure model to span all possible compositions for the envelope between the two extremes of solar ($Z_{\rm ices}$ = 0.01) to 100% H_2O/ices ($Z_{\rm ices}$ = 1), and varying amounts of rocky cores to envelope ratios. We show the results at a nominal age of 4.6 Gyr for GJ 1214b and at 8 Gyr for Kepler-11e in the ternary diagrams that relate Earth-like nucleus, water/ices, and H/He by mass (see Figure 8). Each ternary diagram corresponds to a specific planetary mass, and every point in the ternary diagram depicts one unique composition. These ternary diagrams are equivalent to the (x, y, z)-plane where $x + y + z = 1$, and $x, y, z > 0$. The values for the transit radius are shown in color in terms of Earth radii and the lines of constant radii are labeled. There are a few important aspects to note from the results contained in these ternary diagrams.

1. The presence of H/He considerably increases the transit radius. We find that all detected low-mass planets with a measured mass, that have an envelope, and that happen to have an equilibrium temperature warmer than 500 K (Kepler-11b,c,d,e,f, Kepler-18b, Kepler-20b, 55Cnc-e, Kepler-68b, Kepler-36c, and Kepler-30b) have a radius no larger than five times that of the Earth. This suggests (see isoradius lines in Figure 8) that the H/He content is limited to less than ∼20% by mass for hot sub-Neptunes (less than 10 $M_\oplus$). In fact, if we remove Kepler-11e and Kepler-30b from the list of planets, we find that the rest of the low-mass transiting

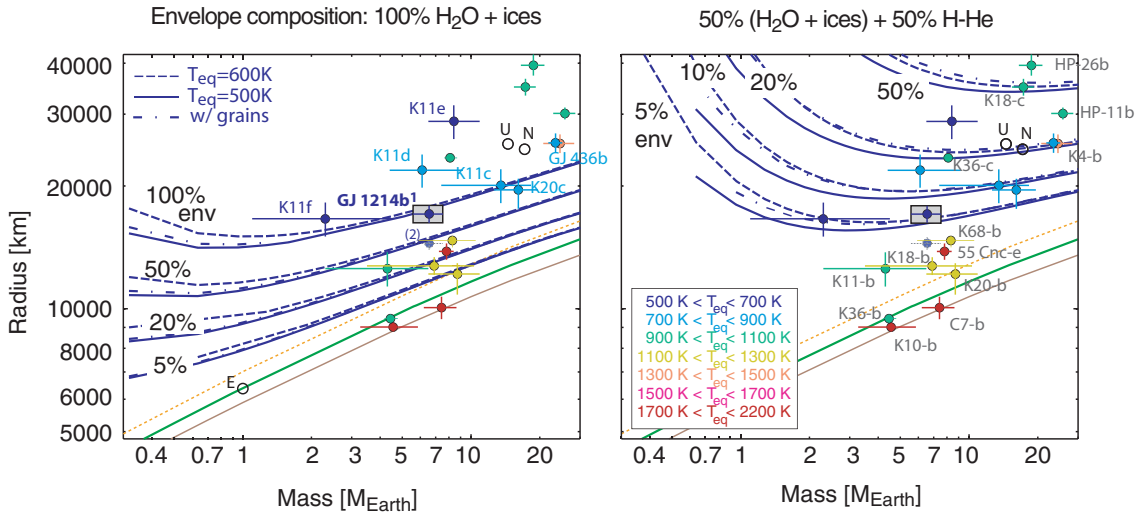

Figure 7. Mass–radius relationships for sub-Neptunes. The relationships between mass and radius for planets with an Earth-like nucleus below envelopes of varying mass fraction (100%, 50%, 20%, 10%, and 5%) are shown for a grain-free atmosphere at $T_{eq} = 500$ K (solid blue), and $T_{eq} = 600$ K (dashed blue), and a grainy atmosphere at $T_{eq} = 500$ K (dash-dotted blue). Two envelope compositions are shown: 100% H_2O/ices (left) and with 50% (H_2O/ices)+50% H/He (right). These MR relationships apply only to the planets GJ 1214b, Kepler-11e, Kepler-11f, Kepler-30b, and GJ 3470b as their equilibrium temperatures are ∼560 K, ∼650 K, ∼575 K, ∼600 K, and almost 700 K, respectively. The MR relationships shown correspond to an age of 4.6 Gyr. Planets are color coded by their equilibrium temperatures (calculated for an albedo of zero and an atmospheric redistribution factor of 1/4). Uranus and Neptune are shown for reference. The mass–radius relationships for three rocky compositions are shown: an Earth-like composition (green), a Mercury-like—enriched in iron with respect to Earth with an iron to silicate ratio six times that of Earth—(brown), and one voided of iron completely (pure magnesium-silicate oxides, orange). The latter shows the limit above which a planet has to have volatiles and cannot be completely rocky.

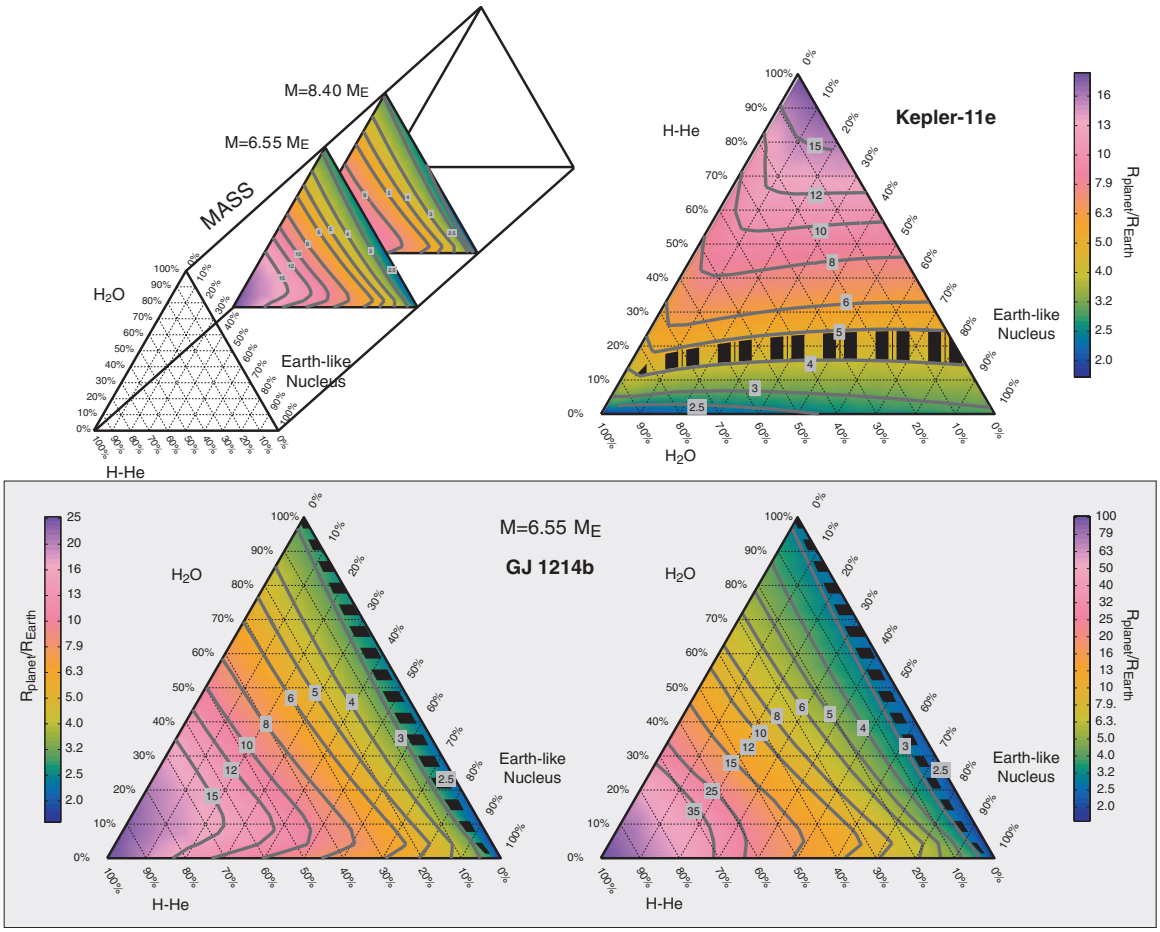

Figure 8. Ternary diagrams for GJ 1214b and Kepler-11e. These triangular diagrams relate the composition χ in terms of Earth-like nucleus fraction, water+ices fraction, and H/He fraction to total mass, to the radius for a specific planetary mass. Each vertex corresponds to 100%, and the opposite side to 0% of a particular component. The color bar shows the radius in terms of Earth radii, and the gray lines are the isoradius curves labeled in terms of Earth radii. The collection of ternary diagrams for a range of planetary masses forms a triangular prism (top left). The black band shows the compositions constrained by data for GJ 1214b for a grain-free envelope (bottom left), and a grainy envelope (bottom right), and Kepler-11e for a grain free envelope (top right) as projected onto the planetary mass M from the ternary diagrams at $M + \Delta M$ and $M - \Delta M$ (where ΔM are the uncertainty values taken from the observational data).

planets so far, with a measured mass, have a maximum of 10% by mass of H/He. Given the bias toward measuring bigger masses, it remains to be determined if there is a population of planets hidden in the *Kepler* candidates with radius 4–5 R_E that have more H/He content.

2. The radius is most sensitive to the amount of H/He and much less to the amount of H_2O/ices and rocky nucleus. This is seen from how parallel the lines of constant radius are to increasing amounts of H/He content. This means that with a radius measurement and just some knowledge that the planetary mass ranges between 5 and 10 $M_\oplus$, it is possible to estimate the H/He content of the planet. Conversely, even with perfect data for mass and radius, it is not possible to estimate the amount of water/ices or refractory material, as they trade off quite efficiently.
3. The effect of the presence of grains is nonlinear and most noticeable for planets with large contents of H/He.

The possible compositions for GJ 1214b that take into account the uncertainty in mass and radius are shown with a black band in the bottom panel of Figure 8. It is clear that this planet has less than 10% by mass of H/He, but that it can have a wide range of compositions because of the trade-off between water/ices and rocky nucleus. Another way to show the results is depicted in Figure 9, where the trade-off between bulk H/He and rocky nucleus (middle figure) or bulk H/He and H_2O/ices (bottom figure) is shown. This can be translated to the content of H/He and H_2O/ices in the atmosphere (top of Figure 9). As the amount of the solid core increases, the percentage of H/He in the envelope increases while that of water decreases. This translates to a bulk H/He content that increases as the solid core increases up to a point where it decreases again. The maximum amount of bulk H/He the planet may have happens in conjunction with some water in the envelope.

We show the range in compositions of the envelope admitted by the data at the two limiting ages of 3 Gyr (dash-dotted lines) and 10 Gyr (solid lines) to examine the effect of age. In general, an older planet would admit more H/He than a younger planet for a given radius. For GJ 1214b, the fact that the age is not well constrained does not constitute a problem when inferring the composition of its envelope, as the effect is small. For planets older than ∼1 Gyr with water-dominated envelopes, age has an effect of less than 1% in the inference of envelope composition. We conclude that while the total amount of H/He in GJ 1214b can be robustly constrained to be less than 7% by mass, the data admit almost all possible compositions for the envelope at any given age. In the scenario of a solar metallicity envelope (H/He + $z = 0.01$), we find that the data constraints the content to be ∼3% by mass.

According to their transmission spectra, Bean et al. (2010, 2011) suggest an atmosphere of more than 70% water. If we assume that the upper atmosphere has the same composition as the envelope below, this range would slightly narrow the composition of the planet to have a rocky component of less than 90% by mass (see the top panel of Figure 9). In summary, because of the large trade-offs between refractory material and water/ices, even with spectroscopic measurements and the assumption that the atmosphere is well mixed, it is not possible to sufficiently narrow the refractory or water/ices composition of the planet.

Previous studies. Our maximum content for H/He agrees with both Rogers & Seager (2010b) and Nettelmann et al. (2011) despite having different treatments. Rogers & Seager (2010b) considered three compositions: a four-layer model with

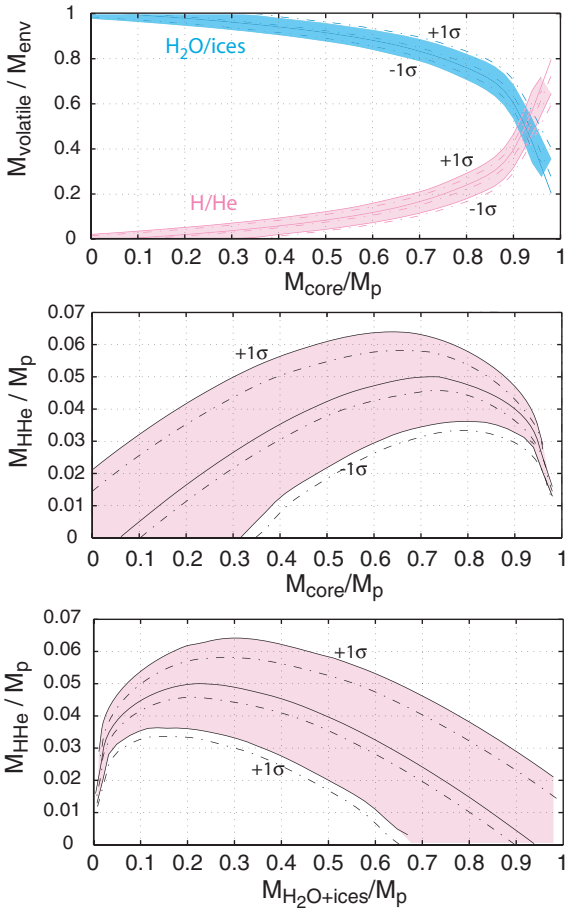

Figure 9. Composition of GJ 1214b. We fit the mass and radius of GJ 1214b including the 1σ uncertainty to estimate the content of H/He, H_2O+ices, and rocky nucleus. Each of the three sets of lines corresponds to the combinations $M+\Delta M$, $R-\Delta R$, M, R, and $M-\Delta M$, $R+\Delta R$, for an old age of the system of 10 Gyr (solid lines, and shaded region) and a younger age of 3 Gyr (dash-dotted lines). Bottom: trade-off between the bulk amount of H/He and water+ices by mass; middle: trade-off between the bulk amount of H/He and rocky nucleus by mass; top: proportion of H–He and water+ices in the envelope as a function of rocky nucleus.

H/He above an ice layer, above an Earth-like nucleus of silicate mantle above an iron core, or a three-layer model with vapor or outgassed H_2 above an Earth-like nucleus. In their four-layer model they find a range of 10^{-4} to 0.068 for H/He is admitted by the data at the 1σ level, in their three-layer model with vapor they find a range of 47%–100%, and with outgassed H_2 a small value of only 5×10^{-4}. While we agree on the maximum amount of H/He and water (for obvious reasons), we find a different value for the minimum amount of water if there is no H/He. Our calculations show a minimum value of 65% (see the bottom panel of Figure 9). A possible explanation for this discrepancy is that the opacity treatment from Rogers & Seager (2010b), which uses the Planck means from molecular line data from F08, does not extend to very water-rich atmospheres. On the other hand, Nettelmann et al. (2011) considered a similar structure to ours with a homogeneous gas envelope. A minor difference that should not influence the results is that they model a homogeneous rocky interior, while we consider a layered Earth-like one below the envelope. In their models of H/He envelope above a rocky core they claim a range of 1.3%–3.4% of H/He. They suggest that the upper limit of H/He can rise up to 5%–6% if the envelope contains 60%–90% water in mass. In comparison, we obtain a value of 3% of H/He envelope at

3 Gyr, and also obtain a maximum amount of H/He by adding 80%–90% by mass of water to the envelope (corresponding to 25% of water by total planetary mass). We suggest that this small difference may come from different opacity values as well.

In addition, we find that our results are robust to reasonable variations of thermal inertia of the planet including different radioactive heat production or heat capacity of the Earth-like nucleus. The lower boundary heat flux entering the envelope is $\dot{L}_{\rm sol} = \dot{\epsilon}_{\rm rad} + C_v dT/dt$, where $\dot{\epsilon}_{\rm rad}$ is the radioactive heat production, and C_v is the heat capacity. We used a chondritic value for the heat generation (2×10^{20} J s^{-1} g^{-1}) which is a factor of ~2 lower than Earth's bulk silicate value, and a heat capacity of 7×10^7 J K^{-1} g^{-1} which is appropriate for the Earth (Stacey 1981). By increasing $\dot{\epsilon}_{\rm rad}$ by a factor of five we find a discrepancy at 3 Gyr of ~2%, and by increasing C_v by a factor of 10 we find a discrepancy of ~6% for a planet with an H/He envelope that makes 3% and 20% of the planet. Being that H/He envelopes are the ones more susceptible to changes in temperature, we conclude that the radius of a sub-Neptune planet is not very sensitive to the thermal evolution of its rocky nucleus. This stands in contrast to the findings by Nettelmann et al. (2011) and Lopez et al. (2012).

3.2. Mass Loss

It is well recognized that atmospheric escape may play an important role in highly irradiated exoplanets (Valencia et al. 2010), and GJ 1214b is no exception. Although a detailed study is beyond the scope of this paper, we can estimate the order-of-magnitude effect of atmospheric escape on GJ 1214b. Starting from the commonly used energy-limited escape formulation (Watson et al. 1981), the mass lost per unit time of a planet of mass M is

$$\dot{M} = \pi \epsilon R_{\rm XUV}^2 R\, F_{\rm XUV}/GMK_{\rm tide}, \quad (5)$$

where $R_{\rm XUV}$ is the radius at which the bulk of the X-ray and extreme-UV (XUV) flux is absorbed, R is the radius below which molecules are bound to the planet, $F_{\rm XUV}$ is the XUV flux at the planet's location, G is the gravitational constant, $K_{\rm tide}$ is a correction factor that takes into account that the molecules only need to reach the Roche lobe before they escape (Erkaev et al. 2007), and ϵ is the heating efficiency defined as the ratio of the net heating rate to the rate of stellar energy absorption. One conservative, simple, and commonly used approach is to assume $R_{\rm XUV} \sim R$. In reality the height at which the planet absorbs X-rays and the XUV are different and also larger than the planetary radius (Lammer et al. 2003). By adopting the assumption, we can simplify Equation (5) to $\dot{M} = 3\epsilon F_{\rm XUV}/4G\rho K_{\rm tide}$ where ρ is the density of the planet, which increases with time as the planet loses mass. Mass loss progresses from fast early on, to slow as time increases, due to two facts: (1) the lighter outer regions get stripped away, leaving a denser planet from which molecules have a harder time escaping, and (2) the XUV flux from the star decreases with time.

The most unconstrained parameter, and where most of the physics is hidden in the mass-loss equation, is the heating efficiency, although common values range between 0.1 and 0.4. Finally, it is important to know how the XUV flux of the star has varied over time, and while GJ 1214 is considered to be a quiet star currently (Charbonneau et al. 2009), being a low-mass M star, it most likely had an active period early on. We implement the model of XUV flux proposed by Ribas (2010). The XUV luminosity starts in a saturated phase after which it drops off as a power-law function of age. The saturation phase duration (t^*) depends on the type of star, as seen by its bolometric luminosity. If we focus on a conservative estimate we can further simplify the mass-loss equation by assuming that the planet loses mass at the present density held constant. This is obviously an idealization and a lower bound for estimating the amount of mass lost, since at a young age planets are lighter and less capable of binding their upper atmospheres. We also set $K_{\rm tide} = 1$. The expression for the XUV flux (Ribas 2010) is

$$F_{\rm XUV} = \begin{cases} 4.04 \times 10^{-24}\, L_{\rm bol}^{0.79}\, a^{-2}\ ({\rm erg^{-1}\ s^{-1} cm^{-2}}) & \text{if } t_9 < t_9^*, \text{ and} \\ 29.7\, t_9^{-1.72} a^{-2}\ ({\rm erg^{-1}\ s^{-1} cm^{-2}}) & \text{if } t_9 > t_9^* \end{cases} \quad (6)$$

where $t_9^* = 1.66 \times 10^{20}\ L_{\rm bol}^{-0.64}$ in Gyr. We use a value of $L_{\rm bol} = 0.00328\, L_{\rm Sun}$ (Charbonneau et al. 2009) and obtain a saturation phase duration of 2 Gyr for GJ 1214b. We calculate a mass loss between 100 Myr and 3 Gyr of 0.6 $M_{\rm E}$ and 2.5 $M_{\rm E}$ for a heating efficiency of 0.1 and 0.4, respectively. This corresponds to a planet losing 9% or 27% of its mass, respectively. This will affect the composition and structure of the planet. This is most important when trying to assess the origin of the planet and the stability of an envelope. Charbonneau et al. (2009) estimated through a hydrodynamic calculation that it would take 700 Myr to lose an envelope of H/He that makes 5% of the planet's mass. According to our simple calculation, the current flux at the planet's semi-major axis is 39 W m^{-2}, and the present mass-loss rate is $2.4 \times 10^8 \epsilon$ kg s^{-1} or $\sim 1.25\epsilon$ Earth-masses per billion years. If the heating efficiency is close to 1, then a modest envelope ($\gtrsim 0.2\, M_p$) may be stable for a billion year timescale. Without a detailed calculation of atmospheric escape that includes the effects of a mixed atmosphere, it is unclear how stable or vulnerable a thin envelope may be. On the other hand, our simple calculation more robustly suggests that the compositional cases, where GJ 1214b has a modest envelope, seem to be stable. Therefore, while atmospheric escape might have been significant in the past, it appears to be moderate at present for GJ 1214b.

3.3. Comparison to Kepler-11

A good starting point to compare low-mass planets is GJ 1214b, because it is the coolest volatile planet and lies right at the threshold of a pure water mass–radius relationship. This means that any volatile planet over 1 Gyr old, as cool as or colder than GJ 1214b with a radius comparable to or larger than GJ 1214b necessarily has H/He. Even though the planets shown in Figure 7 have different ages, they are all older than 1 Gyr, with CoRoT-7b being the youngest (1.2–2.3 Gyr; Léger et al. 2009), so that the MR relationships apply. In fact, most of the transiting planets with known mass are older than the solar system, so the inferred amount of H–He from a younger age (of 4.6 Gyr) would be a minimum.

From Figure 7 we infer that Kepler-11f also has some H/He in its envelope, despite its very low mass of $(2.0–0.9) \pm 0.8\, M_\oplus$ (Lissauer et al. 2011) as its radius stands above the pure-water relationship adequate for its equilibrium temperature. In fact, because of the behavior of the mass–radius relationships for volatile compositions that flare out toward low masses, both planets Kepler-11f and GJ 1214b could have the same composition. This flaring effect is due to the fact that low-mass planets have low gravities that do not bind efficiently their volatile envelopes.

Furthermore, we focus on Kepler-11e as this planet is as cool as GJ 1214b but its radius is 1.6 times larger. We obtain all possible compositions for Kepler-11e (top left, Figure 8) with the new reported data in Lissauer et al. (2013) and find that the minimum amount of bulk H/He is 10% and the maximum is 18% by mass (an improvement from the old reported radius (Lissauer et al. 2011) that yielded 10%–25% content). Being that this planet is the largest and coolest of the transiting super-Earths, it means that all other detected volatile planets have less than 20% bulk H/He. In fact, we find that all volatile super-Earths discovered so far have less than 10% H/He by mass, comparable to Uranus and Neptune (Hubbard & MacFarlane 1980), except for Kepler-11e and Kepler-30b. We find the latter to have between 5% and 15% H/He. This also brings into light that the solar system trend of decreasing H/He with heliocentric distance for the gaseous planets (Hubbard & MacFarlane 1980) does not apply to the Kepler-11 system.

A study by Lopez et al. (2012) investigated the possible compositions for each planet of the Kepler-11 system with an evolutionary model and connected it to atmospheric escape histories. For the structure part, they considered the envelope to be made of an outer layer of H/He above an interior water layer. They use a non-gray model for their atmosphere and opacities at 50 times solar for all their models. For water-less worlds they report that present-day (at 8 Gyr) inventories of H/He are 17.2% for Kepler-11e, and less than ∼8% for all other planets. This stands in excellent agreement with our results considering that the amount of H/He would increase somewhat once they take into account the 1σ uncertainty in masses and radii.

Placing constraints on the amount of H/He helps validate formation models. According to our model, GJ 1214b must have formed rather early, when there was still enough H/He in the solar nebula. In addition, multi-planet systems pose an additional constraint, which is to explain either the trend or lack thereof of H/He content with heliocentric distance. The latter is the case of Kepler-11, with planet e having to have at least 10% of H/He and up to 18% at 42 $R_{\rm Sun}$, and neighboring planets d at 34 $R_{\rm Sun}$ and low-mass planet f at 44 $R_{\rm Sun}$ with at most 10% H/He. A study by Ikoma & Hori (2012) investigates the formation of single low-mass planets with H/He envelopes by invoking in situ accretion that they then apply to Kepler-11. While they do not consider H/He+H_2O mixtures for envelopes which would have an effect on the rate of cooling and accretion due to higher opacities, they explain the H/He content of most of the planets in the system. It remains to be shown how accretion of low-mass multiple planets can acquire envelopes that also have water/ices.

4. SUMMARY AND CONCLUSIONS

To assess the bulk composition of low-mass, low-density exoplanets and specifically GJ 1214b, we ran a comprehensive suite of internal structure and evolutionary models with a proposed prescription for opacity values that span from solar to about 450 times solar—corresponding to a composition of 100% H_2O/ices.

Given that the opacity tables that are commonly used by internal structure models are only known at discrete metallicity values that do not cover all the possible envelope compositions that the sub-Neptune planets may have, we focused our efforts in fitting these opacity tables to an analytical function that describes the global behavior of opacities in the pressure–temperature (P–T) and metallicity regime (from water/ices) in which they are derived, as well as extrapolate smoothly into higher P–T and water content space. The most important regimes for opacities for warm sub-Neptune planets (with an equilibrium temperature ∼500 K) are up to ∼5 kbar and ∼2000 K, which covers the radiative–convective boundary in the envelope. Opacities at larger pressures (with corresponding larger temperatures) fall within the fully convective interior.

Interestingly, we find that the differences in opacity values of a pure water/ices envelope and a 50× solar envelope, which is one of the most metal-rich opacity tables available and corresponds to 1/3 water/ices + 2/3 H/He, are not too large, on the order of a few dex. This means that while using it for envelopes with much larger water contents is not consistent, it probably does not introduce a big source of error in the results.

We find that there is another type of degeneracy pertinent to sub-Neptune planets that arises from the evolutionary history of the planet. Two different envelope compositions of the same mass around the same rocky nucleus may yield the same radius at a given age while differing in the rest of their evolutionary tracks. This degeneracy is different in character to the one that arises from the trade-offs between the different compositional end members.

We obtain the bulk composition of GJ 1214b and find that no more than 7% of H/He is needed to explain the radius of this planet given its mass. In addition, based on formation arguments we expect to have some H/He present in the envelope. This is due to the fact that some refractory material is expected to compose this planet (from the condensation sequence). Our result is consistent with two previous studies focused on GJ 1214b, which use different treatments for the opacities.

More generally, we find that the radius of low-density planets with a mass between 5 and 10 $M_\oplus$ is most sensitive to the amount of H/He, and much less on the amount of water and rocks. On the upside, this means that it is possible to place good constraints on the amount of H/He in these planets, which can be used to further constrain formation models. On the down side, it means that little can be said about the amount of water or rocks in these planets because these two compositional end members trade off very efficiently.

For GJ 1214b and similar planets, the implication is that the inference of a water-rich upper atmosphere from transmission spectroscopy studies does not help constrain the bulk composition of the envelope and planet, whereas an H/He dominated atmosphere would restrict the bulk composition much more, only if we assume a homogeneous composition between the upper atmosphere and deeper envelope.

Furthermore, we find that almost all discovered low-mass planets—Kepler 11b,c,d,f, Kepler-18b, Kepler-20b, 55Cnc-e, Kepler-68b, Kepler-36c—have a maximum H/He component of less than 10% by mass. While it could be that some of them have no H/He whatsoever, it seems that, despite having much hotter equilibrium temperatures, the low-density, low-mass exoplanets share a similar trait to Neptune and Uranus of having a few percent of H/He. The exceptions are Kepler-11e and Kepler-30b with a range of 10%–18% and 5%–15% of bulk H/He, respectively. Being that there is a bias toward detecting larger planets, the fact that the majority of the low-mass planets have less than 10% H/He indicates that larger contents are probably not common. The tightly packed Kepler-11 system seems to have a range of H/He that does not vary monotonically with heliocentric distance, with planets d and f having less H/He than planet e, which may point to more local/planet-specific conditions determining the compositional outcome. In

other words, it remains to be explained why Kepler-11e acquired 10%–18% by mass of H/He while simultaneously its inner and outer neighbors acquired less. Multiplanet sub-Neptune systems with known H/He contents may prove to be key in understanding planet formation.

Inferring the bulk composition of low-mass planets helps us clarify the differences in nature between the solid super-Earths and the sub-Neptune planets that share the same mass range, and also provide useful constraints to formation and migration scenarios for this new class of planets.

This work was performed (in part) under contract with the California Institute of Technology (Caltech) funded by NASA through the Sagan Fellowship Program executed by the NASA Exoplanet Science Institute. We thank Ignasi Ribas for his comments on the XUV fluxes of stars. We thank Jonathan Fortney for his careful and insightful review that has significantly increased the quality of the manuscript.

REFERENCES

Adams, E., Seager, S., & Elkins-Tanton, L. 2008, ApJ, 673, 1160
Alexander, D. R., & Ferguson, J. W. 1994, ApJ, 437, 879
Bean, J. L., Désert, J.-M., Kabath, P., et al. 2011, ApJ, 743, 92
Bean, J. L., Kempton, E., & Homeier, D. 2010, Natur, 468, 669
Berta, Z. K., Charbonneau, D., Bean, J., et al. 2011, ApJ, 736, 12
Charbonneau, D., Berta, Z. K., Irwin, J., et al. 2009, Natur, 462, 891
Croll, B., Albert, L., Jayawardhana, R., et al. 2011, ApJ, 736, 78
Crossfield, I. J. M., Barman, T., & Hansen, B. M. S. 2011, ApJ, 736, 132
de Mooij, E. J. W., Brogi, M., de Kok, R. J., et al. 2012, A&A, 538, A46
Désert, J.-M., Bean, J., Miller-Ricci Kempton, E., et al. 2011, ApJL, 731, L40
Erkaev, N. V., Kulikov, Y. N., Lammer, H., et al. 2007, A&A, 472, 329
Freedman, R. S., Marley, M. S., & Lodders, K. 2008, ApJS, 174, 504
Fraine, J. D., Deming, D., Gillon, M., et al. 2013, ApJ, 765, 127
French, M., Mattsson, T. R., Nettelmann, N., & Redmer, R. 2009, PhRvB, 79, 054107
Guillot, T. 2010, A&A, 520, A27
Guillot, T., & Morel, P. 1995, A&A, 109, 109
Hubbard, W. B., & MacFarlane, J. J. 1980, JGR, 85, 225
Ikoma, M., & Hori, Y. 2012, ApJ, 753, 66
Lammer, H., Selsis, F., Ribas, I., et al. 2003, ApJL, 598, L121
Léger, A., Rouan, D., Schneider, J., et al. 2009, A&A, 506, 287
Lissauer, J. J., Fabrycky, D. C., Ford, E. B., et al. 2011, Natur, 470, 53
Lissauer, J. J., Jontof-Hutter, D., Rowe, J. F., et al. 2013, ApJ, 770, 131
Lodders, K. 2003, ApJ, 591, 1220
Lopez, E. D., Fortney, J. J., & Miller, N. 2012, ApJ, 761, 59
Miller-Ricci, E., & Fortney, J. J. 2010, ApJL, 716, L74
Nettelmann, N., Fortney, J. J., Kramm, U., & Redmer, R. 2011, ApJ, 733, 2
Ribas, I. 2010, in IAU Symp. 264, Solar and Stellar Variability: Impact on Earth and Planets, ed. A. G. Kosovichev, A. H. Andrei, & J.-P. Rozelot (Cambridge: Cambridge Univ. Press), 3
Rogers, L. A., & Seager, S. 2010a, ApJ, 712, 974
Rogers, L. A., & Seager, S. 2010b, ApJ, 716, 1208
Saul, A., & Wagner, W. 1989, JPCRD, 18, 1537
Saumon, D., Chabrier, G., & van Horn, H. M. 1995, ApJS, 99, 713
Stacey, F. D. 1981, in Evolution of the Earth, ed. R. J. O'Connell & W. S. Fyfe (Washington, DC: AGU), 272
Valencia, D., Ikoma, M., Guillot, T., & Nettelmann, N. 2010, A&A, 516, A20
Valencia, D., O'Connell, R. J., & Sasselov, D. D. 2006, Icar, 181, 545
Valencia, D., Sasselov, D. D., & O'Connell, R. J. 2007, ApJ, 665, 1413
Vinet, P., Rose, J., Ferrante, J., & Smith, J. 1989, JPCM, 1, 1941
Wagner, F. W., Tosi, N., Sohl, F., Rauer, H., & Spohn, T. 2012, A&A, 541, A103
Watson, A. J., Donahue, T. M., & Walker, J. C. G. 1981, Icar, 48, 150